Possibility of Doping $CuGaSe_2$ *n*-Type by Hydrogen

Miaomiao Han,[1,*] Peter Deák,[2,†] Zhi Zeng,[3] and Thomas Frauenheim[2,4]

[1] *School of Science, Huzhou University, Huzhou, Zhejiang 313000, China*
[2] *Bremen Center for Computational Material Science, University of Bremen, Bremen D-28344, Germany*
[3] *Key Laboratory of Materials Physics, Institute of Solid State Physics, HFIPS, Chinese Academy of Sciences, Hefei 230031, China*
[4] *Computational Science Research Center (CSRC) Beijing and Computational Science and Applied Research (CSAR) Institute Shenzhen, No.10 East Xibeiwang Road, Haidian District, Beijing 100193, China*

(Received 21 December 2020; revised 4 February 2021; accepted 11 March 2021; published 12 April 2021; corrected 4 May 2021)

Copper-indium-gallium-selenide (CIGS) alloys are successfully applied in thin-film solar cells. For a better use of the solar spectrum, they also offer the possibility of multijunction devices by tuning the composition in the different layers. As-grown CIGS is intrinsically *p*-type due to copper vacancies (V_{Cu}), but *n*-type doping is also useful for applications. While $CuInSe_2$ can be easily turned *n*-type, $CuGaSe_2$ cannot, and this represents a problem, because increasing the band gap of CIGS requires a high Ga/In ratio. Investigating the effect of hydrogen on $CuGaSe_2$ by an optimized hybrid functional, we show that hydrogenation from an atomic source as, e.g., by a hydrogen plasma treatment, can turn the material *n*-type due to the formation of shallow donor V_{Cu}+2H complexes, while H_2 implantation, producing an internal hydrogen reservoir, can be used to produce semi-insulating material. We also show that under normal process conditions, unintentional hydrogen incorporation does not have a significant effect on $CuGaSe_2$.

DOI: 10.1103/PhysRevApplied.15.044021

I. INTRODUCTION

The usage of photovoltaic solar energy is increasing in recent years. The second generation of thin-film solar cells based on Cu(In, Ga)(Se, S)$_2$, or CIGS for short, has achieved a record efficiency of 23.3% [1,2], and is one of the main competitors to silicon cells with respect to efficiency and cost. In addition, CIGS is also advantageous for application in multijunction solar cells, since the gap of the different layers can be tuned by varying the ratio of In and Ga, and/or S and Se. Point defects and impurities, which may act as dopants, traps, or recombination centers, play a critical role in the photovoltaic properties of the material [3–7]. CIGS alloys are intrinsically *p*-type, however, $CuInSe_2$ can easily be doped *n*-type while effective *n*-type doping of $CuGaSe_2$ is apparently not possible [8]. Theoretical calculations confirm that *n*-type doping by substitution on cation or anion sites in $CuGaSe_2$ is not feasible [9]. This may pose a problem in an alloy where a high Ga/In ratio is needed to increase the gap.

Hydrogen is often used to passivate dangling bonds in semiconductors to eliminate the associated traps (e.g., amorphous silicon solar cells do not even work without approximately 10% H content) [10,11], but it can also be used to passivate dopants to create semi-insulating material [12,13]. Hydrogen may also provide shallow levels, compensating the intentional dopants or even change the type of conductivity, as proposed, e.g., in $CuInSe_2$ [14]. Considering this versatility of hydrogen, it is helpful to explore its effect in CIGS materials systematically. Here we investigate that in $CuGaSe_2$. Such a study should consider both the effect of unintentional contamination and also the active introduction of hydrogen for defect engineering. Hydrogen may get incorporated into CIGS unintentionally during growth (because the applied CdS buffer layer usually has a high hydrogen content), in nonvacuum processing steps, or during heat treatment or rapid thermal annealing in H_2 (to remove oxygen and improve material quality) [15–18]. It can be introduced intentionally, e.g., by implantation [19,20] or annealing in a hydrogen plasma. Hydrogen can exist in the crystal as an individual interstitial H atom or as a H_2 molecule, but can also form complexes with native defects and dopants. As a consequence, hydrogen can influence the electrical activity of the intrinsic defects and introduce H-related donors or acceptors as well. All that may affect the intrinsic *p*-type behavior, therefore, a systematic and detailed study of H-related defects in $CuGaSe_2$ is necessary to explore the possibility of changing the conductivity to *n*-type.

*mmhan@zjhu.edu.cn
†deak@uni-bremen.de

 © 2021 American Physical Society

Earlier, using the local density approximation (LDA) to density-functional theory (DFT), Kiliç and Zunger found [14,21] that H passivates the copper vacancy (V_{Cu}), which is the main shallow acceptor in intrinsic CIGSe, and that interstitial H is a deep negative-U defect. They also predicted that hydrogenation of the defect complex between two copper vacancies and a cation antisite, $(2V_{Cu}+In_{Cu})^0$, gives rise to a shallow donor, which makes $CuInSe_2$ n-type. In contrast, they found the complex of $(2V_{Cu}+Ga_{Cu})^0$ with hydrogen to be a deep donor in $CuGaSe_2$, and no n-type doping by hydrogenation of this material. It should be noted though that the decoration of the remaining dangling bonds of V_{Cu} with H atoms have not been considered (only the addition of H_2 molecules to V_{Cu}+H) [21], while vacancies in other semiconductors can accommodate up to four H atoms [22], and the arising defects may be electrically active [23]. Hydrogenation of the antisites has not been investigated either, even though they influence the carrier concentration [9,24].

Here, we study the effect of H on all relevant defects in $CuGaSe_2$ (CGSe) with an optimized hybrid functional, which reproduces the band gap and complies with the generalized Koopmans theorem (GKT), thereby allowing for an accurate determination of defect levels [25]. We find that the antisites can be partially or fully passivated by one or two hydrogen atoms, respectively. A single hydrogen atom can fully passivate the V_{Cu} acceptor, however an additional H atom turns it into a shallow donor, while further hydrogenation of V_{Cu} is not favored energetically. We calculate the charge transition levels of all intrinsic defects before and after hydrogenation, and use those to determine the position of the Fermi level, considering different methods of hydrogenation. We find that hydrogen does not get easily incorporated during usual process steps, but hydrogen implantation can produce semi-insulating material, while a hydrogen plasma treatment (providing H atoms as a source for hydrogenation) can turn $CuGaSe_2$ n type.

Our paper is organized as follows. The computational framework is introduced in Sec. II A, while, Sec. II B describes the choice of chemical potentials for the calculation of the formation energies. Section III describes the H-related defects, their charge transition levels, and their effect on the equilibrium position of the Fermi level, based on the calculated formation energies. The conclusions are drawn in Sec. IV.

II. COMPUTATIONAL FRAMEWORK

A. Methods

Figure 1 shows the 16-atom, body-centered, tetragonal conventional cell of CGSe, as well as the $2 \times 2 \times 2$ supercell (with 128 atoms), which we use for defect calculations. In this system, the cations are tetrahedrally coordinated by four Se atoms, and the anions are surrounded by two Cu and two Ga atoms.

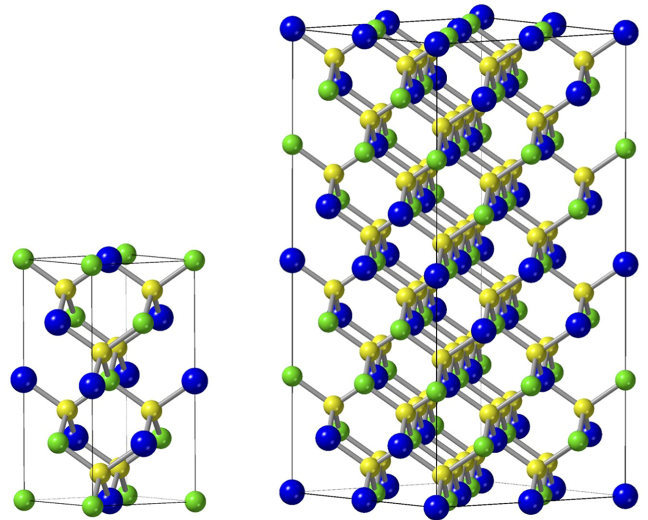

FIG. 1. The 16-atom and 128-atom cell of $CuGaSe_2$. Cu, blue; Ga, green; Se, yellow spheres.

Calculations are carried out by the Vienna *ab initio* simulation package, VASP 5.3.5 [26–28]. The projector augmented wave (PAW) method is applied [29,30] and the Ga3d electrons are treated as part of the core, since our tests show that they have negligible effects on the band gap. (The Cu3d electrons are, of course, treated in the valence shell.) A 400- (800-) eV cutoff is applied for the expansion of the wave functions (charge density). All geometries are relaxed until the forces on every atom are less than 0.02 eV/Å. Defect calculations are carried out with spin polarization.

The standard implementations of DFT, as LDA or generalized gradient approximation (GGA), underestimate the band gap. The Heyd-Scuseria-Ernzerhof hybrid functional [31,32], with the standard parametrization (HSE06), increases the gap but in CIGS it still underestimates it and does not comply with the GKT, i.e., with the independence of the Kohn-Sham energy levels from their occupation [33]. If the double criterion of reproducing the gap (proper derivative discontinuity of the total energy as a function of the occupation number) and satisfying the GKT (linear behavior between two integer numbers) are met, highly accurate defect levels can be obtained [34–36]. It has been shown that simultaneously tuning the two parameters of a HSE(α,μ) functional (where α and μ are the mixing and screening parameter, respectively), the two conditions can be fulfilled [25,37]. Such a functional mimics the exact density functional, guaranteeing high accuracy in the ionization energies and in the localization of states [38]. Our previous work has shown that HSE(0.26,0.08) is optimal for $CuGaS_2$ [39]. The optimal parameters are generally material dependent, however, we find that the parameters

optimized for $CuGaS_2$ are transferable to $CuGaSe_2$. As shown in Table I, using HSE(0.26,0.08) the GKT is satisfied within 0.02 eV in $CuGaSe_2$ too, and the band gap of 1.76 eV also appears to be appropriate, considering the experimental optical gap of 1.73 eV at 77 K [43,44]. (The fulfillment of the GKT is checked for the donor level of the relaxed neutral Sn_{Ga} defect in a 128-atom supercell with experimental lattice parameters [45].) The accuracy of this functional has been validated by comparison to the experimentally observed, Ga_{Cu}-related photoluminescence band in $CuGaSe_2$ [39], as shown also within the Supplemental Material [46], where the effect of optimization is also demonstrated.

We use this optimized hybrid to determine the equilibrium lattice parameters of the primitive cell, with a $6\times6\times6$ Monkhorst-Pack (MP) k-point set [48], performing constant volume relaxations and then fitting to Murnaghan's equation of state [49,50]. Defect calculations are all carried out using these equilibrium lattice parameters ($a = 5.646$ Å, $c = 11.044$ Å) in the 128-atom supercell, with the Γ approximation for Brillouin-zone sampling.

The formation energy of a defect in charge state q is calculated as [51,52]

$$\Delta E^q_{\text{form}}(\text{defect}) = E^q_{\text{defect}} + E^q_{\text{corr}} - E_{\text{host}} - \sum_i n_i\mu_i + q(E_F - E_V + \Delta V_{\text{align}}), \quad (1)$$

where E^q_D and E_{host} are the calculated total energy of the supercell with and without defect, n_i is the number of atoms, of type i, introduced into the supercell when forming the defect, and μ_i is their chemical potential. E_F–E_V is the Fermi energy, referenced the VBM in the bulk. ΔV_{align} is the potential alignment between the neutral defect and the perfect cell, and E^q_{corr} is the energy correction required for charged defects in a periodic model [53]. Charge corrections for the total energy are obtained by using the method of Freysoldt, Neugebauer, and Van de Walle [54], while localized defect levels are corrected using the relation, $e^q_{\text{corr}} = -2E^q_{\text{corr}}/q$, derived by Chen and Pasquarello [55]. For these corrections the directional average of the experimental high-frequency dielectric constant ε_∞ (7.47 for $CuGaSe_2$) [56] is used, both for vertical (fixed ions) and adiabatic (relaxed ions) charge transitions. In principle, in the latter case the static dielectric constant ε_0 should be used, however, earlier we observe that in cases where $\varepsilon_0 \gg \varepsilon_\infty$, much too shallow adiabatic charge transition levels are obtained this way, while using ε_∞ reproduces the experimental values better [31,57,58]. The explanation probably is that a relatively large supercell describes a substantial part of the ionic screening explicitly, and using the bulk value of ε_0 amounts to double counting.

Assuming thermodynamic equilibrium, the concentration of the defects in their different charge states can be estimated from the calculated formation energies, and by solving the neutrality equation for the Fermi energy:

$$N_C\exp\left(-\frac{E_C - E_F}{kT}\right) + \sum_i |q_i|N^q_{Ai} = N_V\exp\left(-\frac{E_F - E_V}{kT}\right) + \sum_i |q_i|N^q_{Di}, \quad (2)$$

where E_C–E_F is the Fermi-level position with respect to the conduction-band minimum(CBM), N^q_{Di} and N^q_{Ai} are the concentration of (all types of) ionized donors and acceptors, respectively, as determined by their formation energy (i.e., neglecting entropy effects):

$$N^q_{Ai,Di} = N_0\exp\left[-\frac{\Delta E^q_{\text{form}}(Ai, Di)}{kT}\right]. \quad (3)$$

N_C (N_V) is the effective volume-density of states at the conduction- (valence-) band edge, and N_0 is the density of defect sites in the crystal for the given defect [59]. Since the concentration of charged defects is dependent on the Fermi level through the formation energy, Eqs. (1)–(3) have to be solved self-consistently in an iterative procedure. We set the temperature to 750 K, which is a typical temperature for annealing $CuGaSe_2$ [19].

B. Stability region

The formation energy of defects depends on the chemical potential of the elements and of the electrons (Fermi

TABLE I. Calculated band gaps of 128-atom $CuGaS_2$ and $CuGaSe_2$ supercells, compared to experiment, and the Koopmans test for Sn_{Ga} with HSE(0.26,0.08).

	E_g(calc.)	E_g(expt.)	$KS_{HOMO}(N)$	E_N–E_{N-1}	KS_{LUMO} $(N-1)$
$CuGaS_2$	2.55	2.53 (2 K) [40–42]	−1.55	−1.56	−1.57
$CuGaSe_2$	1.76	1.73 (77 K) [43,44]	−0.90	−0.89	−0.87

The Kohn-Sham level of the occupied defect state (HOMO) in the neutral system, KS_{HOMO}(N), and of the unoccupied defect level (LUMO) in the positive charged state, $KS_{LUMO}(N-1)$, are compared to the self-consistently calculated electron-removal energy (at fixed geometry), E_N–E_{N-1}. All three are referenced to the conduction-band minimum and given in eV. Fulfillment of the GKT requires all three values to be equal.

TABLE II. Energy of the atoms (E_A) calculated by HSE(0.26,0.08), the experimental atomization energy ($-E_{\text{coh}}$), and the corresponding chemical potential μ_i^{standard} used in this work. All values in eV.

	E_A	$-E_{\text{coh}}^{58}$	μ^{standard}
Cu	−0.71	3.49	−4.20
Ga	−0.86	2.82	−3.68
Se	−2.41	2.44	−4.85
H	−1.77	2.26	−4.03

energy) as given in Eq. (1). The chemical potential of element i in a reservoir is expressed as $\mu_i = \mu_i^{\text{standard}} + \Delta\mu_i$, where μ_i^{standard} is the chemical potential in the standard chemical state and $\Delta\mu_i$ is the deviation from that under given experimental conditions. The HSE hybrid does not work well for metals and must be optimized for each semiconductor separately, therefore, to obtain μ_i^{standard}, we calculate the energy of the atoms with HSE(0.26,0.08), and then deduct the experimental atomization energy (negative of the cohesion energy) [60]. Table II shows the values we use.

$\Delta\mu_i$ can be varied to reflect specific conditions. In thermal equilibrium, however,

$$\Delta\mu_{\text{Cu}} + \Delta\mu_{\text{Ga}} + 2\Delta\mu_{\text{Se}} = \Delta H_f^{\text{CuGaSe}_2}. \tag{4}$$

To avoid the precipitation of elemental solids, the chemical potentials should be bound by

$$\Delta\mu_{\text{Cu}} \le 0\,;\ \Delta\mu_{\text{Ga}} \le 0\,;\ \Delta\mu_{\text{Se}} \le 0. \tag{5}$$

The chemical potentials are further restricted by the formation of unwanted competing binary phases like GaSe, CuSe, Cu_2Se, Cu_3Se_2, and the ordered defect compound Cu_5GaSe_8. The chemical potential region, where $CuGaSe_2$ is stable, is shown in Fig. 2 with light-blue shading. To set up the phase diagram, we use the experimental formation enthalpies of the compounds (see Table III), because, again, the hybrid optimized for $CuGaSe_2$ may not be optimal for the other compounds.

In Fig. 2 three points are specified, to represent Cu-poor (A), Ga-poor (B) and Se-poor (C) conditions. These are used for discussing defect physics. Since high-efficiency $Cu(In,Ga)Se_2$ absorbers are generally prepared under a highly selenium-rich atmosphere, it is instructive to interpret the defect physics for this material under selenium-rich conditions on the Se-$Cu(In,Ga)Se_2$ phase boundary in the stability diagram (between A and B points). In addition, the chemical potential of copper between A and B agrees well with the measured value of −0.5 to −0.7 eV in high-quality Se-rich $Cu(In,Ga)Se_2$.

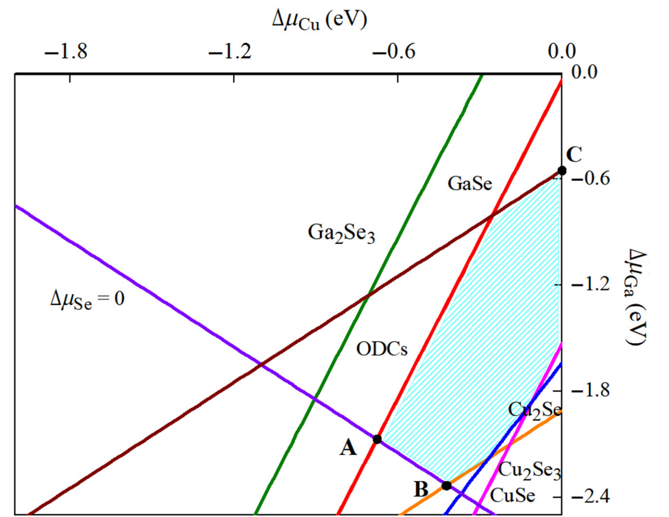

FIG. 2. Stability diagram for $CuGaSe_2$, as derived from the data in Table II. The chemical potentials of Cu, Ga, and Se at point A are (−0.68, −2.07, 0), at B (−0.42, −2.33, 0) and at C (0, −0.55, −1.1), respectively. All values in eV.

III. RESULTS

To study the effect of hydrogen on $CuGaSe_2$, we investigate H_i and H_{2i} interstitials as well as the complexes of hydrogen with the most abundant intrinsic defects, (V_{Cu}+nH), (Ga_{Cu}+nH), and (Cu_{Ga}+nH). For a single hydrogen atom, four interstitial starting positions are considered: the Cu—Se and the Ga—Se bond-center (BC) site, as well as the tetrahedral sites surrounded by cations (TC) or anions (TA). As shown in Fig. 3, for H^- the global energy minimum is at the so-called antibonding (AB) site, behind a Cu atom, while H^+prefers the BC site between Cu and Se.

It can be inferred that H^+ behaves as a cation, bonding to the anion Se, while H^- behaves as an anion, preferentially binding to the more electronegative cation Cu. These ionic bonds are quite strong, so H^0 is always less stable than either H^-_{AB} or H^+_{BC}. Neutral hydrogen placed into V_{Cu} moves to bind with a Se neighbor [Fig. 3(c)].

Ga_{Cu} is a double donor [24,39], so hydrogen binds to it as an anion in the AB position, while Cu_{Ga} is a double

TABLE III. Experimental formation energies of the compounds relevant to the stability diagram.

Compound	ΔH_f
$CuGaSe_2$	−2.75 [61]
GaSe	−1.65 [62]
CuSe	−0.42 [61]
Cu_2Se	−0.61 [61]
Cu_3Se_2	−1.03 [63]
Cu_5GaSe_8	−10.96 (HSE06)

All values in eV.

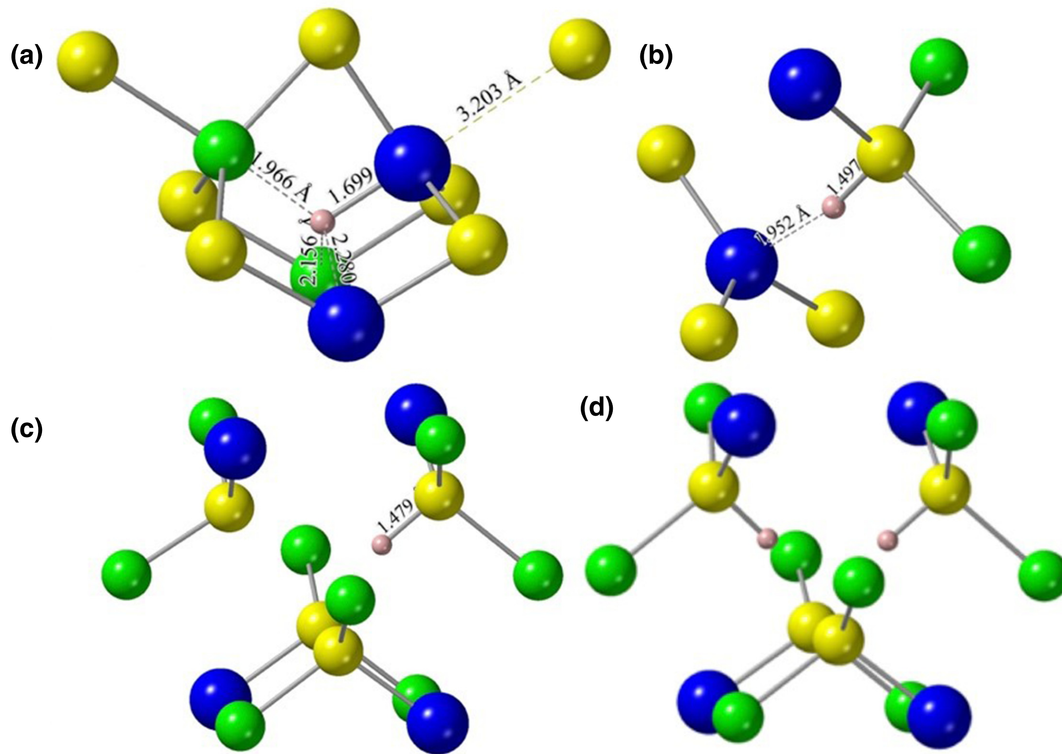

FIG. 3. Stable configuration for the (a) negative (H_{AB}^-) and (b) positive (H_{BC}^+) interstitial, as well as for the (c) V_{Cu}+H and (d) V_{Cu}+2H defects. Cu, blue; Ga, green; Se, yellow spheres.

acceptor [24,39], so hydrogen behaves as a cation going to the BC site again and binding to the Se neighbor of Cu_{Ga}, as shown in Fig. 4. As a consequence, the double donor and the acceptor are partially passivated, becoming a single donor and acceptor, respectively. Using simple electron-counting arguments it is easy to see that Ga_{Cu}+H is a shallow donor. Out of the three electrons, which the four Se neighbors would (nominally) donate to copper, and the three electrons of Ga_{Cu}, four are used to create the four bonds of Ga_{Cu} (to its three Se neighbors and to H_{AB}), the fifth turns the dangling bond of the fourth Se neighbor into a lone pair orbital (deep in the VB), and the remaining electron finds only place on the CBM. This is confirmed by the actual calculation.

For H_{2i}, we consider the H_2 molecule at the TA and TC sites, as well as the $H_{BC}H_{AB}$ (also called H_2^*) complex [64,65], with H_{AB}^- bonded to Cu and H_{BC}^+ bonded to Se (Se—H...Cu—H), which is an electrically passive defect. As it turns out, H_{2i} at the TC site is preferred energetically by far.

As can be seen in Fig. 3(c), the three other Se dangling bonds of V_{Cu}+H offer the possibility of further hydrogen uptake. Since the acceptor V_{Cu} is electrically passivated by a single hydrogen, addition of further H atoms may turn it into a donor. Using electron-counting again, in the case of V_{Cu}+2H, two Se dangling bonds are saturated by the hydrogens, while the other two become lone pair orbitals (deep in the VB) accommodating two of the three electrons the four Se neighbors would (nominally) donate to copper. The third electron is forced onto CBM here too. This is confirmed by the actual calculation. Further hydrogenation would only place more electrons onto the CBM, so that is energetically not favorable, as we indeed find.

When Ga_{Cu}+H forms, Ga_{Cu}—Se bond gets broken [see Fig. 4(a)]. One would expect that upon adding one more H atom, a $H_{BC}H_{AB}$-type defect (with H_{BC} bonded to Se) will form. However, a complex of $(Ga_{Cu}+H)^+$ and a H_{AB}^- interstitial behind a next-neighbor Ga site [see Fig. 5(a)] is energetically more favorable, because the donor electron of Ga_{Cu}+H is transferred to the interstitial H. This way Ga_{Cu}+H is passivated and further hydrogen atoms would go to remote interstitial sites. Cu_{Ga}+H offers the possibility of inserting an additional H_{BC}^+ to bond with another Se neighbor of Cu_{Ga}, as shown in Fig. 5(b). With that the antisite defect is fully passivated and the increasing lattice strain makes adding further hydrogens energetically unfavorable.

Having obtained the stable defect configurations, we calculate their charge transition levels, which determine their electrical activity. These are summarized in Fig. 6. Interstitial H is found to exhibit a negative-U behavior with a (+/−) level at 1.33 eV above the VBM, which is

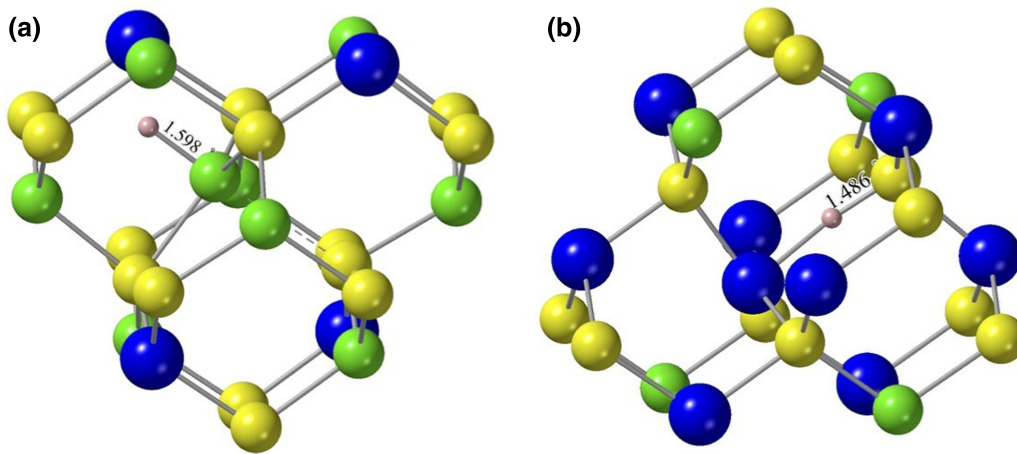

FIG. 4. Ga_{Cu}+H (a) and the Cu_{Ga}+H (b) complexes in the neutral charge state.

more or less the same as in previous calculations [14,66]. Interstitial H_{2i} is electrically inactive. The single acceptor V_{Cu} is passivated by hydrogen, so the V_{Cu}+H complex is electrically inactive as well. As explained above, however, an additional hydrogen turns it into a shallow effective-mass-like (EMT) single donor. Cu_{Ga} is a double acceptor with charge transition levels (0/−1) at 0.3 eV and (−1/−2) at 1.0 eV above the VBM. The Cu_{Ga}+H complex [Fig. 4(b)] is a deep single acceptor with a (0/−1) level at $E_V + 0.7$ eV. Adding the second hydrogen leads to complete passivation. Ga_{Cu}, is a deep double donor with charge transition levels (+2/+) at 1.0 eV and (+/0) at 1.3 eV. The Ga_{Cu}+H complex is, again a shallow EMT donor, as explained above. In the Ga_{Cu}+2H complex shown in Fig. 5(a), the donor electron is transferred to the H_{AB}-Ga part resulting in an electrically inactive defect.

As can be seen from Fig. 6, hydrogen can give rise to shallow donor levels (V_{Cu}+2H, Ga_{Cu}+H) as well as to electron and hole traps (Cu_{Ga}+H, H_i) in CGSe, so it may influence the carrier concentration. The end effect depends on the relative concentrations. According to Eq. (1), the formation energy of H-related defects depends on the hydrogen chemical potential, which has to be chosen to reflect the conditions under which hydrogen is introduced into CGSe.

First we consider annealing in H_2, which is usually carried out between 600–850 K at 1 atm, to improve crystal quality [19,20]. The chemical potential of hydrogen in an external reservoir of H_2 molecules can be calculated at a given temperature and pressure, as [67]

$$\begin{aligned}\mu_H = \frac{1}{2}\{&E(\mathrm{H_2}) + 8.617386\times 10^{-5}T \\ &\times \ln[1.267865\times 10^3 pT^{-(7/2)}(1-e^{-(6.301215\times 10^3/T)})] \\ &+ 0.2715\}.\end{aligned} \tag{6}$$

Using this chemical potential, however, has not resulted in a significant hydrogen incorporation, so we may conclude that annealing in H_2 under usual condition has no effect on the carrier concentration in CGSe.

Next, following Ref. [21], we consider internal reservoirs. (Hydrogen, introduced under nonequilibrium conditions, can form internal reservoirs of H in the crystal.) Hydrogen, incorporated during growth, saturates dangling bonds of vacancies and grain boundaries [15,16]. To simulate that, we choose the energy of hydrogen in the V_{Cu}+H complex, $\mu_H = E(V_{Cu}+\mathrm{H}) - E(V_{Cu})$, as a possible chemical potential of the internal reservoir. Hydrogen can also be introduced by implantation of H^+ or $H_2{}^+$ions [68,69], with most of the hydrogen likely ending

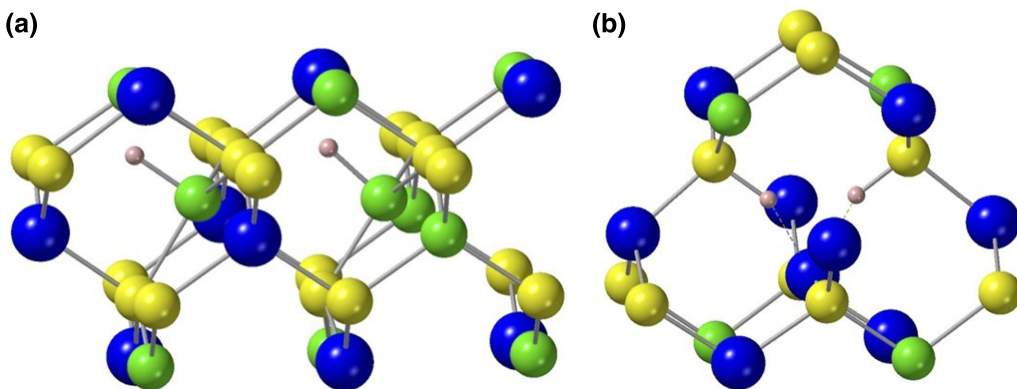

FIG. 5. Complexes Ga_{Cu} +2H (a) and Cu_{Ga}+2H (b).

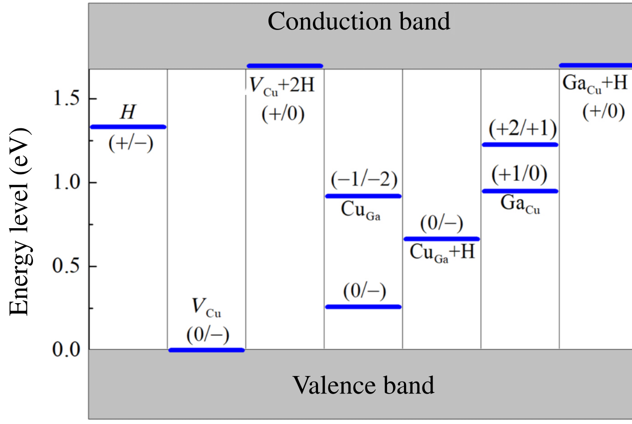

FIG. 6. Charge transition levels of the electrically active defects in hydrogenated $CuGaSe_2$.

up as interstitial H_{2i}. So as, an alternative for the chemical potential of the internal reservoir, we choose $\mu_H = (1/2)[E(H_{2i}) - E_{host}]$.

Hydrogen plasma treatment is a very effective way of introducing hydrogen into semiconductors [70–74]. The plasma discharge dissociates H_2 molecules and provides an external source of atomic hydrogen ($H^+ + e^-$). Therefore, we also investigate atomic hydrogen as an external reservoir, at the usual plasma temperature and pressure. For that, we set [66]

$$\mu_H = E(H) + 8.617386 \quad (7)$$

$$\times 10^{-5} T \ln(19.313058 \times p T^{-(5/2)}) \quad (8)$$

at $T = 700$ K and $p = 1$ kPa.

Using these μ_H values, as well as the charge transition levels of Fig. 6, we calculate the formation energies according to Eq. (1) and solve Eqs. (1)–(3) by using the program of Buckerdige [75]. The results for the equilibrium Fermi-level position are shown in Table IV for the stoichiometric conditions marked A, B, and C in Fig. 2.

TABLE IV. Fermi-level position with respect to the VBM in intrinsic CGSe (considering only V_{Cu}, Ga_{Cu}, and Cu_{Ga}, as the most abundant defects), and after hydrogen incorporation, assuming V_{Cu}+H and H_{2i} as an internal reservoir, or hydrogen atoms in the gas phase (at 700 K and 1 kPa) as external reservoir for hydrogen.

H reservoir	A (Cu poor)	B (Ga poor)	C (Se poor)
None	0.07	0.20	0.53
V_{Cu}+H	0.14	0.21	0.53
H_{2i}	0.84	0.81	0.84
H atoms at 700 K, 1 kPA	1.54	1.21	1.55

All values in eV. The stoichiometric conditions, A, B, and C, of Fig. 2 are considered.

As can be seen, hydrogen incorporation during growth (with V_{Cu}+H being the reservoir) has little effect on the Fermi-level position. Therefore, considering also our result regarding H_2 annealing, unintentional H incorporation will not influence the Fermi level in CGSe much. In contrast, annealing after hydrogen implantation (H_{2i} being the internal reservoir) will result in semi-insulating material with the Fermi level around midgap. Hydrogen plasma treatment provides an external reservoir of atomic hydrogen. As Table IV shows, equilibrium with an external reservoir of atomic hydrogen pushes the Fermi level up, near to the conduction-band edge, making CGSe n-type. For the temperature (700 K) and pressure (1 kPa) considered here, electron concentrations will be in the order of 10^{18} cm^{-3} in Cu- and Se-poor, and 10^{16} cm^{-3} in Ga-poor samples. Therefore, a hydrogen plasma treatment (i.e., an external source of atomic hydrogen) is not only the most effective way for hydrogenation but leads to n-type conductivity. The mechanism of that can be understood based on Fig. 7, which shows the formation energies of all defects, with respect to atomic H as an external reservoir.

The negative formation energies of the neutral (electrically inactive) H_{2i}, V_{Cu}+H, and Cu_{Ga}+2H defects show that atomic hydrogen is not stable with respect to molecule formation or against saturating dangling bonds (both leading to energy gain with respect to atomic hydrogen in the external reservoir). These results show, how an internal reservoir of hydrogen arises, but they do not mean an infinite hydrogen uptake. On the one hand, the number of dangling-bond defects is limited. On the other, while H_{2i} can be abundant (just as in silicon) [69,70], with increasing concentration the formation energy (given here in the solute limit) also increases, due to the increasing elastic strain, and that sets a limit to solubility. (It should be noted, that the Boltzmann statistics, used in Eqs. (1)–(3), also assumes noninteracting defects.)

In fact, under p-type conditions, the shallow donor V_{Cu}+2H becomes dominant over H_{2i}, as can be seen in Fig. 7. These defects diminish also the concentration of V_{Cu} acceptors and overcompensate the hole concentration provided by the rest. The position of the Fermi level is primarily determined by V_{Cu} and V_{Cu}+2H under Cu- and Se-poor conditions (A and C, respectively), while under Ga-poor conditions (B) by the Cu_{Ga}+H acceptors and the V_{Cu}+2H donors. (The defects Ga_{Cu}+H and H_{AB} have relatively high formation energies, while H_{2i}, V_{Cu}+H, Cu_{Ga}+2H and Ga_{Cu}+2H are neutral and inactive.) The Fermi level is pinned at 1.54, 1.21, and 1.55 eV, under Cu-, Ga-, and Se-poor conditions. These values all mean a Fermi-level position above midgap, making CGSe n-type. In the Cu- and Se-poor cases, the Fermi level is close enough to the conduction band to give rise to a reasonably high concentration of free electrons. Therefore, hydrogenation of Cu- or Se-poor CGSe by providing atomic hydrogen as an external source, e.g., by

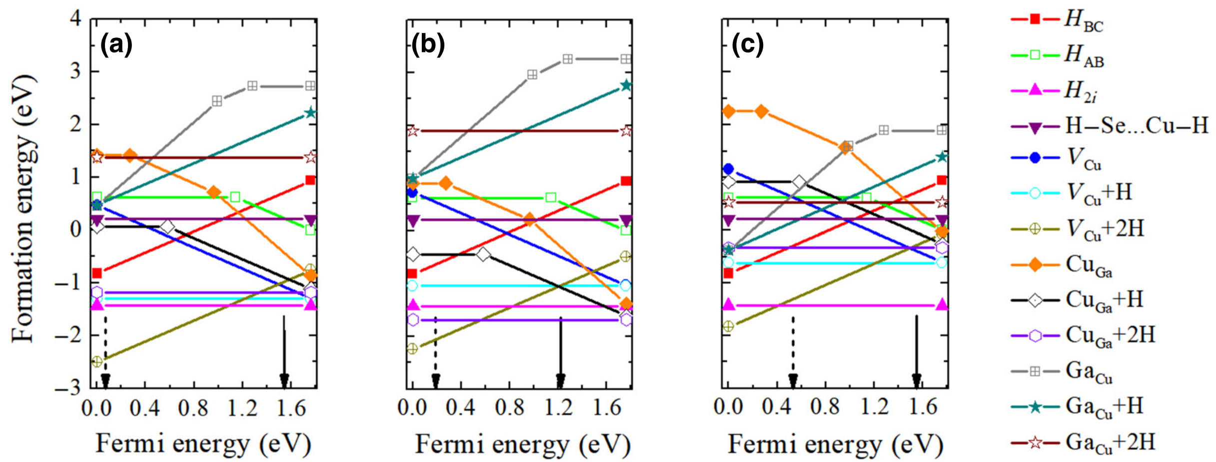

FIG. 7. Formation energies of the intrinsic and H-related defects in $CuGaSe_2$ assuming the stoichiometric conditions A (Cu poor), B (Ga poor), and C (Se poor), as described in Fig. 2. Atomic H is taken as external hydrogen reservoir. The dashed and the solid arrow show the Fermi level in native and in H-doped $CuGaSe_2$.

a H-plasma treatment, could be used to produce *n*-type conductivity.

IV. SUMMARY

We perform a systematic computational study of the effect of hydrogen on $CuGaSe_2$. We find that besides interstitial H_i and H_{2i}, hydrogen can form a defect complex with the most abundant native defects V_{Cu}, Cu_{Ga}, and Ga_{Cu}. Our most useful finding is that hydrogen does not only passivate intrinsic defects but can produce shallow donor states as well. This affects the position of the Femi level, i.e., the type of conductivity. We show that hydrogen does not get easily incorporated during usual process steps, but hydrogen implantation can produce semi-insulating material, while a hydrogen plasma treatment (providing for atomic hydrogen) can turn $CuGaSe_2$ *n*-type, mainly by the formation of shallow donor V_{Cu}+2H defects. The *n*-type doping by hydrogen is more effective under Cu- or Se-poor conditions and less in Ga-poor material.

ACKNOWLEDGMENTS

This work is financially supported by the National Natural Science Foundation of China under Grant No. 61804154. The supercomputing service from AM-HPC and from the Supercomputer Center of Northern Germany (HLRN Grant No. hbp00054) is acknowledged.

[1] Solar Frontier Achieves: World Record Thin-Film Solar Cell Efficiency of 23.35%. http://www.solar-frontier.com/eng/news/2019/0117_press.html.

[2] P. Jackson, R. Wuerz, D. Hariskos, E. Lotter, W. Witte, and M. Powalla, Effects of heavy alkali elements in Cu(In, Ga)Se_2 solar cells with efficiencies up to 22.6%, Phys. Status Solidi RRL **10**, 583 (2016).

[3] G. Leibfried and N. Breuer, *Point Defects in Metals I: Introduction to the Theory, Springer Tracts in Modern Physics* (Springer-Verlag, New York, 1978).

[4] P. Deák, in *Computational Materials Science, NATO Science Series III*, edited by R. Catlow and E. Kotomin (IOS Press, Amsterdam, 2003), Vol. 187, p. 255.

[5] C. G. Van de Walle and J. Neugebauer, First-principles calculations for defects and impurities: Applications to III-nitrides, J. Appl. Phys. **95**, 3851 (2014).

[6] A. Alkauskas, P. Deák, J. Neugebauer, A. Pasquarello, and C. G. Van de Walle, *Advanced Calculations for Defects in Materials* (Wiley, New York, 2011).

[7] C. Freysoldt, B. Grabowski, T. Hickel, J. Neugebauer, G. Kresse, A. Janotti, and C. G. Van de Walle, First-principles calculations for point defects in solids, Rev. Mod. Phys. **86**, 253 (2014).

[8] J. H. Schön, E. Arushanov, N. Fabre, and E. Bucher, Transport properties of n-type $CuGaSe_2$, Solar Energy Mater. & Solar Cells **61**, 417 (2000).

[9] C. L. Bailey, L. Liborio, G. Mallia, S. Tomic, and N. M. Harrison, Defect physics of $CuGaS_2$, Phys. Rev. B **81**, 205214 (2010).

[10] C. G. V. de Walle, Energies of various configurations of hydrogen in silicon, Phys. Rev. B **49**, 4579 (1994).

[11] B. Aradi, P. D. A. Gali, J. E. Lowther, N. T. Son, E. Janzen, and W. J. Choyke, Ab initio density-functional supercell calculations of hydrogen defects in cubic SiC, Phys. Rev. B **63**, 245202 (2001).

[12] M. Stutzmann and J. Chevallier, *Hydrogen in Semiconductors*, ISBN 978-0-444-89138-9 (North Holland, Amsterdam, 1991).

[13] J. I. Pankove and N. M. Johnson, *Hydrogen in Semiconductors*, ISBN: 9780080864310 (Academic Press, San Diego, 1991).

[14] Ç Kiliç and A. Zunger, Doping of chalcopyrites by hydrogen, Appl. Phys. Lett. **83**, 2007 (2003).

[15] N. Maticiuc, A. Katerski, M. Danilson, and M. Krunks, XPS study of OH impurity in solution processed CdS thin films, Sol. Energy Mater. Sol. Cells **160**, 211 (2017).

[16] J. B. Varley and V. Lordi, Electrical properties of point defects in CdS and ZnS, Appl. Phys. Lett. **103**, 102103 (2013).

[17] V. Kapur, A. Bansal, P. Le, and O. Asensio, Non-vacuum processing of $CuIn_{1-x}Ga_xSe_2$ solar cells on rigid and flexible substrates using nanoparticle precursor inks, Thin Solid Films **53**, 431 (2003).

[18] T. Matsumoto, Y. Miyaji, K. Kiuchi, and T. Kato, Chloride multi-source epitaxial growth of $CuGaS_2$ and $CuGaSe_2$, Jpn. J. Appl. Phys. **32**, 142 (1993).

[19] A. Duchatelet, T. Sidali, N. Loones, G. Savidand, E. Chassaing, and D. Lincot, 12.4% efficient $Cu(In, Ga)Se_2$ solar cell prepared from one step electrodeposited Cu − In − Ga oxide precursor layer, Sol. Energy Mater. Sol. Cells **119**, 241 (2013).

[20] H. Miyazaki, R. Mikami, A. Yamada, and M. Konagai, Efficiency improvement of $Cu(InGa)Se_2$ thin film solar cells with a high Ga composition using rapid thermal annealing, Jpn. J. Appl. Phys. **43**, 4244 (2004).

[21] C. Kiliç and A. Zunger. Phys. Rev. B **68**, 075201 (2003).

[22] E. V. Lavrov, J. Weber, L. Huang, and B. Bech Nielsen, Vacancy-hydrogen defects in silicon studied by Raman spectroscopy, Phys. Rev. B **64**, 035204 (2001).

[23] G. Thiering and A. Gali, Complexes of silicon, vacancy, and hydrogen in diamond, Phys. Rev. B **92**, 165203 (2015).

[24] J. Pohl and K. Albe, Intrinsic point defects in $CuInSe_2$ and $CuGaSe_2$ as seen via screened-exchange hybrid density functional theory, Phys. Rev. B **87**, 245203 (2013).

[25] P. Deák, M. Lorke, B. Aradi, and T. Frauenheim, Optimized hybrid functionals for defect calculations in semiconductors, J. Appl. Phys. **126**, 130901 (2019).

[26] G. Kresse and J. Furthmüller, Efficient iterative schemes for ab initio total-energy calculations using a plane-wave basis set, Phys. Rev. B **54**, 11169 (1996).

[27] G. Kresse and J. Furthmüller, Efficiency of ab-initio total energy calculations for metals and semiconductors using a plane-wave basis set, Comput. Mater. Sci. **6**, 15 (1996).

[28] G. Kresse and J. Hafner, Ab initio molecular-dynamics simulation of the liquid-metalamorphous-semiconductor transition in germanium, Phys. Rev. B **49**, 14251 (1994).

[29] P. E, Blöch, projector augmented-wave method, Phys. Rev. B **50**, 17953 (1994).

[30] G. Kresse and D. Joubert, From ultrasoft pseudopotentials to the projector augmented-wave method, Phys. Rev. B **59**, 1758 (1999).

[31] J. Heyd, G. E. Scuseria, and M. Ernzerhof, Erratum: 'hybrid functionals based on a screened Coulomb potential, J. Chem. Phys. **124**, 219906 (2006).

[32] J. Heyd, G. E. Scuseria, and M. Ernzerhof, Hybrid functionals based on a screened Coulomb potential, J. Chem. Phys. **118**, 8207 (2003).

[33] S. Lany and A. Zunger, Polaronic hole localization and multiple hole binding of acceptors in oxide wide-gap semiconductors, Phys. Rev. B **80**, 085202 (2009).

[34] P. Deák, A. Gali, B. Aradi, and T. Frauenheim, Accurate gap levels and their role in the reliability of other calculated defect properties, Phys. Stat. Sol. (b) **248**, 790 (2011).

[35] P. Deák, B. Aradi, T. Frauenheim, E. Janzen, and A. Gali, Accurate defect levels obtained from the HSE06 range-separated hybrid functional, Phys. Rev. B **81**, 153203 (2010).

[36] P. Deák, B. Aradi, and T. Frauenheim, Polaronic effects in TiO_2 calculated bu the HSE06 hybrid functional: Dopant passivation by carrier self-trapping, Phys. Rev. B **83**, 155207 (2011).

[37] P. Deák, Q. D. Ho, F. S. B. Aradi, M. Lorke, and T. Frauenheim, Choosing the correct hybrid for defect calculations: A case study on intrinsic carrier trapping in $\beta\text{-}Ga_2O_3$, Phys. Rev. B **95**, 075208 (2017).

[38] Y. Chen, Z. Chen, and W. Yang. Chem. Phys. Lett. **11**, 23 (2020).

[39] M. Han, Z. Zeng, T. Frauenheim, and P. Deák, Defect physics in intermediate-band materials: Insights from an optimized hybrid functional, Phys. Rev. B **96**, 165204 (2017).

[40] C. Bellabarba, J. Gonzalez, and C. Rincon, Optical-absorption spectrum near the exciton band edge in $CuGaS_2$, Phys. Rev. B **53**, 7792 (1996).

[41] B. Tell, J. L. Shay, and H. M. Kasper, Electrical properties, optical properties, and band structure of $CuGaS_2$ and $CuInS_2$, Phys. Rev. B **4**, 2463 (1971).

[42] B. Tell and H. M. Kasper, Excitons and the spin-orbit splitting in $CuGaS_2$, Phys. Rev. B **7**, 740 (1973).

[43] B. Tell and P. Bridenbaugh, Aspects of the band structure of $CuGaS_2$ and $CuGaSe_2$, Phys. Rev. B **12**, 3330 (1975).

[44] M. P. Vecchi, J. Ramos, and W. Giriat, Photoluminescence in $CuGaSe_2$, Solid-State Electron. **21**, 1609 (1978).

[45] S. C. Abrahams and J. L. Bernstein, Piezoelectric nonlinear optic $CuGaS_2$ and $CuInS_2$ crystal structure: Sublattice distortion in AIBIIICVI2 and AIIBIVCV2 type chalcopyrites, J. Chem. Phys. **59**, 5415 (1973).

[46] See Supplemental Material at http://link.aps.org/supplemental/10.1103/PhysRevApplied.15.044021 for the validation of the optimized functional and the effect of optimizing the HSE parameters, which includes Ref. [47].

[47] C. Spindler, D. Regesch, and S. Siebentritt, Revisiting radiative deep-level transitions in $CuGaSe_2$ by photoluminescence, Appl. Phys. Lett. **109**, 032105 (2016).

[48] H. J. Monkhorst and J. D. Pack, Special points for brillonin-zone integrations, Phys. Rev. B **13**, 5188 (1976).

[49] F. Birch, Finite elastic strain of cubic crystals, Phys. Rev. **71**, 809 (1947).

[50] F. D. Murnaghan, The compressibility of media under extreme pressures, Proc. Nat. Acad. Sci. USA **30**, 244 (1944).

[51] A. Zunger, Electronic structure of 3d transition-atom impurities in semiconductors, Solid State Physics **36**, 275 (edited by F. Seitz and D. Turnbul, Academic, New York, 1986).

[52] S. B. Zhang and J. E. Northrup, Chemical Potential Dependence of Defect Formation Energies in GaAs: Application to Ga Self-Diffusion, Phys. Rev. Lett. **67**, 2339 (1991).

[53] H.-P. Komsa, T. T. Rantala, and A. Pasquarello, Finite-size supercell correction schemes for charged defect calculations, Phys. Rev. B **86**, 045112 (2012).

[54] C. Freysoldt, J. Neugebauer, and C. G. V. de Walle, Fully Ab Initio Finite-Size Corrections for Charged-Defect

Supercell Calculations, Phys. Rev. Lett. **102**, 016402 (2009).

[55] W. Chen and A. Pasquarello, Correspondence of defect energy levels in hybrid density functional theory and many-body perturbation theory, Phys. Rev. B **88**, 115104 (2013).

[56] C. Parlak and R. Eryigit, Ab initio volume-dependent elastic and lattice dynamical properties of chalcopyrite $CuGaSe_2$, Phys. Rev. B **73**, 245217 (2006).

[57] P. Deák, B. Aradi, and T. Frauenheim, Quantitative theory of the oxygen vacancy and carrier self-trapping in bulk TiO, Phys. Rev. B **86**, 195206 (2012).

[58] P. Deák, M. Lorke, B. Aradi, and T. Frauenheim, Carbon in GaN: Calculations with an optimized hybrid functional, Phys. Rev. B **99**, 085206 (2019).

[59] P. Deák, A. Gali, B. Aradi, M. Kaviani, T. Frauenheim, and A. Gali, Formation of NV centers in diamond: A theoretical study based on calculated transitions and migration of nitrogen and vacancy related defects, Phys. Rev. B **89**, 075203 (2014).

[60] Y. Zhang, J. R. G. Evans, and S. Yang, Corrected values for boiling points and enthalpies of vaporization of elements in handbooks, J. Chem. Eng. Data **56**, 328337 (2011).

[61] N. Meyer, Ph.D. thesis, Freie Universität Berlin, 2000.

[62] D. Cahen and R. Noufifi, Free energies and enthalpies of possible gas phase and surface reactions for preparation of $CuInSe_2$, J. Phys. Chem. Solids **53**, 991 (1992).

[63] G. Gattow and A. Schneider, Die bildungsenthalpien im system kupfer-selen, Z. Anorg. Allg. Chem. **286**, 296 (1956).

[64] P. Deák and L. C, Snyder: Dihydrogen complexes in silicon, Radiat. Eff. Defects Solids **111–112**, 77 (1989).

[65] K. J. Chang and D. J. Chadi, Diatomic-Hydrogen-Complex Diffusion and Self-Trapping in Crystalline Silicon, Phys. Rev. Lett. **62**, 937 (1989).

[66] J. B. Varley, V. Lordi, T. Ogitsu, A. Deangelis, K. Horsley, and N. Gaillard, Assessing the role of hydrogen in Fermi-level pinning in chalcopyrite and kesterite solar absorbers from first-principles calculations, J. Appl. Phys. **123**, 161408 (2018).

[67] J. E. Northrup, R. D. Felice, and J. Neugebauer, Energetics of H and NH_2 on GaN(1010) and implications for the origin of nanopipe defects, Phys. Rev. B **56**, R4325 (1997).

[68] K. Otte, T. Chasse, G. Lippold, B. Rauschenbach, and R. Szargan, Chemical defect explanation for the effect of post-deposition treatments on $CuInSe_2$, J. Appl. Phys. **91**, 1624 (2002).

[69] K. Otte, G. Lippold, D. Hirsh, R. K. Gebhardt, and T. Chassé, Conductivity type conversion of p-type $CuInSe_2$ due to hydrogenation, Appl. Surf. Sci. **179**, 203 (2001).

[70] A. W. R. Leitch, V. Alex, and J. Weber, Raman Spectroscopy of Hydrogen Molecules in Crystalline Silicon, Phys. Rev. Lett. **81**, 421 (1998).

[71] J. Vetterhöffer, J. Wagner, and J. Weber, Isolated Hydrogen Molecules in GaAs, Phys. Rev. Lett. **77**, 5409 (1996).

[72] Y. M. Strzhemechny, Remote hydrogen plasma doping of single crystal ZnO, Appl. Phys. Lett. **84**, 2545 (2004).

[73] G. Wang, G. Y. Zhao, T. Soga, T. Jimbo, and M. Umeno, Effects of H plasma passivation on the optical and electrical properties of GaAs-on-Si, Japan, J. Appl. Phys. **37**(Part 2, No. 11A), L1280 (1998).

[74] C. G. Van de Walle and J. Neugebauer, Hydrogen in semiconductors, Annu. Rev. Mater. Res. **36**, 179 (2006).

[75] J. Buckeridge, SC-Fermi calculation program. https://github.com/jbuckeridge/sc-fermi

Correction: The sentence preceding Eq. (1) was erroneously omitted during the production process and has been restored. The names of complexes were set improperly during the production process in various locations in text and have been fixed.